International Journal of Pharmaceutics 435 (2012) 93–97

Contents lists available at SciVerse ScienceDirect

International Journal of Pharmaceutics

journal homepage: www.elsevier.com/locate/ijpharm

Fluorescence recovery after photo-bleaching as a method to determine local diffusion coefficient in the stratum corneum

Yuri G. Anissimov[a,*], Xin Zhao[b], Michael S. Roberts[c,d], Andrei V. Zvyagin[b]

[a] School of Biomolecular and Physical Sciences, Griffith University, Qld 4222, Australia
[b] MQ Biofocus Research Centre, Macquarie University, NSW 2109, Australia
[c] Therapeutics Research Centre, School of Medicine, University of Queensland, Australia
[d] School of Pharmacy and Medical Sciences, University of South Australia, SA 5001, Australia

ARTICLE INFO

Article history:
Received 24 December 2011
Received in revised form 23 January 2012
Accepted 24 January 2012
Available online 2 February 2012

Keywords:
Stratum corneum
Lipids
Diffusion coefficient
Rhodamine B
FRAP
Modelling

ABSTRACT

Fluorescence recovery after photo-bleaching experiments were performed in human stratum corneum in vitro. Fluorescence multiphoton tomography was used, which allowed the dimensions of the photo-bleached volume to be at the micron scale and located fully within the lipid phase of the stratum corneum. Analysis of the fluorescence recovery data with simplified mathematical models yielded the diffusion coefficient of small molecular weight organic fluorescent dye Rhodamine B in the stratum corneum lipid phase of about $(3–6) \times 10^{-9}$ cm^2 s^{-1}. It was concluded that the presented method can be used for detailed analysis of localised diffusion coefficients in the stratum corneum phases for various fluorescent probes.

1. Introduction

The stratum corneum (SC) is the main barrier to drug delivery through skin and therefore understanding details of solute transport in SC is an important area of research. The SC is a complex multiphase membrane consisting of layers of corneocytes that are sealed tightly by densely packed lipid layers (Wu et al., 2011). Fundamental parameters describing this transport are values of diffusion coefficients in different phases of the heterogeneous SC, that can be used in in silico models of the SC (e.g. Wang et al., 2006, 2007, for recent review of such models see Mitragotri et al., 2011). These values are generally very difficult to obtain in classical skin penetration experiments (Roberts and Anissimov, 2005), as well as in less common skin desorption experiments (Anissimov and Roberts, 2004, 2009), due to difficulties in assessing the true path-length of solute transport through the SC (Bunge et al., 1999). In this work, we deployed the technique of fluorescence recovery after photobleaching (FRAP) (Braeckmans et al., 2003; Sniekers and van Donkelaar, 2005) realised on a fluorescence multiphoton tomography (FMT) to probe diffusion of organic fluorescent dye Rhodamine B (Rh:B, $MW = 479$, Log $P = 1.95$) in the SC lipid phase. FRAP implemented by means of FMT is capable to realise dimensions of the photo-bleached volume from sub-micron to sub-millimetre in linear dimension. Therefore, this volume can be localised fully within the lipid phase of the SC, allowing determination of the value of local diffusion coefficient. Although FRAP has been used before to assess diffusion coefficients of various fluorescent probes in artificial lipid bilayer systems (Johnson et al., 1996), to our knowledge, the presented technique for the first time determines the diffusion coefficient of a solute in the SC lipid phase using FRAP. Since the artificial lipid phases can potentially have structure and composition different to those of the lipid phase of SC, we believe that this addition to the experimental toolbox of SC transport studies is a significant development. Furthermore, the proposed technique can be further developed, by appropriate choice of a fluorophore and by a proper selection of site of the photobleaching, to study the transport inside corneocytes and across a corneocyte envelope. This development has a potential to further advance the understanding of relative importance of different pathways (Anissimov and Roberts, 2009; Kasting et al., 2003; Keister and Kasting, 1986) on the overall solute transport across SC.

2. Methods

All experiments were performed using FMT based on Zeiss510 (Zeiss, Germany) system with a water-immersion objective lens (63×, N.A. 1.3). Zeiss510 system operated in combination with Mai Tai XF-1 femtosecond pulsed laser with a wavelength tuning range

* Corresponding author. Tel.: +61 7 55528496; fax: +61 7 55528065.
E-mail address: Y.Anissimov@griffith.edu.au (Y.G. Anissimov).

0378-5173/$ – see front matter © 2012 Elsevier B.V. All rights reserved.
doi:10.1016/j.ijpharm.2012.01.055

from 710 to 920 nm. The pulse width was evaluated as <100 fs based on the spectral bandwidth measurement at 80-MHz repetition rate, resulting in the high instantaneous peak power (~100 GW/cm^2) at the focal spot. A femtosecond laser operated at a centre wavelength of 810 nm with power incident at the sample estimated as 33 or 16.5 mW (1% or 0.5% of the total laser output energy which was 3310 mW) was employed as the excitation source. To achieve the photobleaching regime, the laser power was increased to 165 mW. A bandpass filter centred at a wavelength of 560 nm (bandwidth, 60 nm) was used to pass the Rh:B fluorescence to a detector.

2.1. Glycerol experiments

Since SC is a complex, highly heterogeneous structure, it was necessary, first, to establish the FRAP method, including optimisation of various experimental parameters, using a simplified model of homogeneously distributed fluorescence. Rh:B solution in glycerol was chosen as this homogeneous fluorescence model, because glycerol possesses high viscosity that was comparable to that of the skin lipids. This model was also preferred, as it has been described in the literature (Braga et al., 2004). Experiments with glycerol solutions of Rh:B were first performed to establish the depth of the photobleached volume. This depth was determined from the axial point spread function (axial PSF) of the FMT used in all FRAP experiments. In order to determine the axial PSF, a 10-μL sample of 10-μM Rh:B in glycerol solution sealed in an o-ring container on a glass slide was scanned at the boundary of the sample and the glass slide. The resultant fluorescent intensity versus depth curve was then derived to obtain the axial PSF curve. The full width at half maximum (FWHM) of the axial PSF was interpreted as the depth of the photo-bleached volume. The axial PSF was dependent mainly on the N.A. of the microscope objective lens assuming its aberration-free characteristics. FRAP experiments were performed with the 10-μM Rh:B in glycerol samples. The samples of the Rh:B solution in glycerol were positioned between glass slide and the cover slip so that the sample was at least 150-μm thick. Photobleached volume of cylindrical shape was formed in the sample to be located far from the boundaries, close to the middle of the sample. The diameter of the cylindrical photobleached volume was chosen to be of similar dimension to the determined depth of photobleaching. The photobleaching was realised by scanning the volume to be photobleached by gradually increasing the laser power (165, 330 or 495 mW). Scanning the tissue with the high laser power results in permanent destruction of fluorescence (photobleaching) of Rh:B molecules in the photobleached volume. After the photobleaching stops, Rh:B molecules from non-photobleached areas of the sample start to diffuse into the photobleached volume, thus recovering the fluorescent molecule concentration in the volume. The recovery of the fluorescence in the photobleached volume was measured by scanning with a reduced laser power (33 mW).

2.2. FRAP experiment in SC

Pieces of human skin were obtained from one subject and SC prepared using trypsin treatment of heat-separated epidermis, as previously described (Kligman and Christophers, 1963). SC was soaked in 10-μM Rh:B solution in water for 2 days in order to guarantee a steady state concentration distribution of the fluorophore throughout all SC phases. After saturation, the SC sample was removed from the solution and excess solution was wiped with tissue. Then SC was placed between a glass slide and a cover slip and sealed to prevent the drying of the sample. FRAP was conducted at different positions in the SC using the FMT. Significant Rh:B fluorescence was detected only in the lipid phase of the SC, most likely due to the lipophilic nature of the fluorophore. The results for further mathematical analysis were selected by ensuring that the largest possible photobleached volume was all within the lipid phase of the SC. As with the glycerol FRAP experiments, photobleaching of SC was achieved by scanning the volume to be photobleached by gradually increasing the laser power (165 mW). The recovery of the fluorescence in the photobleached volume was measured by scanning with the reduced power (16.5 mW). Both circular and square photobleached areas were used in the SC FRAP experiments. Diameter of the circle and side of the square were selected to be of similar dimension to the depth of the photobleaching.

2.3. Mathematical models and data analysis

Two simple mathematical models are considered: the first (referred to as the 3D-model) is based on the solution of the diffusion equation with the assumption that the diffusion medium around the photobleached volume is infinite. The second model (referred to as the 2D-model) is based on the assumption that the fluorophore diffusion occurs only in the lipid phase of the SC and this phase is an infinite 2D-layer of thickness equal or less than the photobleached volume. This layer is limited by assumed impermeable corneocytes from the top and bottom (this assumption is mathematically identical to the assumption of no fluorophore present in the corneocytes). For both models, it is assumed that the photobleaching is uniform within the photobleached volume (V_{PB}), that is, if $C(\mathbf{x}, t)$ is the fluorophore concentration at the time t and at a position $\mathbf{x} = (x, y, z)$, then immediately after photobleaching occurs, the concentration is:

$$C(\mathbf{x}, 0) = \begin{cases} \alpha C_0 & \text{inside } V_{PB} \\ C_0 & \text{outside } V_{PB} \end{cases} \quad (1)$$

where C_0 is the original concentration of the fluorophore and $0 \le \alpha < 1$ is the degree of photobleaching. The concentration at any time after the photobleaching can be found by solving the diffusion Eq. (2) with initial condition (1).

$$\frac{\partial C(\mathbf{x}, t)}{\partial t} = D\Delta C(\mathbf{x}, t) \quad (2)$$

where D is the diffusion coefficient. The total fluorescence inside the V_{PB} ($F(t)$) can be found as:

$$F(t) = \iiint_{V_{PB}} C(\mathbf{x}, t) d^3\mathbf{x} \quad (3)$$

where we assumed that fluorescence intensity is proportional to the concentration of the fluorophore. 3D-model is assumed in Eq. (3), for 2D-model, the triple integral in Eq. (3) and integrals below need to be replaced with double integrals.

The initial condition for the problem can be simplified by a change of function, so that:

$$C_f(\mathbf{x}, t) = C_0 - C(\mathbf{x}, t) \quad (4)$$

so that initial condition for C_f is:

$$C_f(\mathbf{x}, 0) = \begin{cases} (1-\alpha)C_0 & \text{inside } V_{PB} \\ 0 & \text{outside } V_{PB} \end{cases} = (1-\alpha)C_0 U(\mathbf{x}) \quad (5)$$

where $U(\mathbf{x})$ is defined as:

$$U(\mathbf{x}) = \begin{cases} 1 & \text{inside } V_{PB} \\ 0 & \text{outside } V_{PB} \end{cases} \quad (6)$$

and C_f satisfies the diffusion Eq. (2). The total fluorescence inside V_{PB} can be defined using C_f:

$$F(t) = V_{PB}C_0 - \iiint_{V_{PB}} C_f(\mathbf{x}, t) d^3\mathbf{x} = V_{PB}C_0 - \int_{-\infty}^{\infty}\int_{-\infty}^{\infty}\int_{-\infty}^{\infty} U(\mathbf{x}) C_f(\mathbf{x}, t) dx\, dy\, dz \quad (7)$$

Taking Fourier transform of the diffusion equation and initial condition then solving yields:

$$\hat{C}_f(\mathbf{k}, t) = C_0(1-\alpha)\hat{U}(\mathbf{k})\exp(-\mathbf{k}^2 t) \quad (8)$$

where

$$\hat{C}_f(\mathbf{k}, t) = \int_{-\infty}^{\infty}\int_{-\infty}^{\infty}\int_{-\infty}^{\infty} C_f(\mathbf{x}, t)\exp(i\mathbf{kx})dx\ dy\ dz \tag{9}$$

is the Fourier transform of C_f, and

$$\hat{U}(\mathbf{k}) = \int_{-\infty}^{\infty}\int_{-\infty}^{\infty}\int_{-\infty}^{\infty} U(\mathbf{x})\exp(i\mathbf{kx})dx\ dy\ dz = \iiint_{V_{PB}} \exp(i\mathbf{kx})d^3\mathbf{x} \tag{10}$$

is the Fourier transform of U.

Using Parseval's theorem for Fourier transform:

$$\int_{-\infty}^{\infty}\int_{-\infty}^{\infty}\int_{-\infty}^{\infty} f(\mathbf{x})g(\mathbf{x})dx\,dy\,dz = \frac{1}{(2\pi)^3}\int_{-\infty}^{\infty}\int_{-\infty}^{\infty}\int_{-\infty}^{\infty} \overline{\hat{f}(\mathbf{k})}\hat{g}(\mathbf{k})dk_1\,dk_2\,dk_3$$

in the integral on right hand side of Eq. (7) yields:

$$\int_{-\infty}^{\infty}\int_{-\infty}^{\infty}\int_{-\infty}^{\infty} U(\mathbf{x})C_f(\mathbf{x}, t)dx\ dy\,dz = \frac{1}{(2\pi)^3}\int_{-\infty}^{\infty}\int_{-\infty}^{\infty}\int_{-\infty}^{\infty} \overline{\hat{U}(\mathbf{k})}\,\hat{C}_f(\mathbf{k})dk_1\ dk_2\,dk_3 \tag{11}$$

together with Eq. (8) this gives:

$$\int_{-\infty}^{\infty}\int_{-\infty}^{\infty}\int_{-\infty}^{\infty} U(\mathbf{x})C_f(\mathbf{x}, t)dx\ dy\,dz = \frac{C_0(1-\alpha)}{(2\pi)^3}\int_{-\infty}^{\infty}\int_{-\infty}^{\infty}\int_{-\infty}^{\infty} \left|\hat{U}(\mathbf{k})\right|^2 \exp(-\mathbf{k}^2 t)dk_1\ dk_2\,dk_3 \tag{12}$$

Therefore, the total fluorescence inside V_{PB} can be found as:

$$F(t) = V_{PB}C_0 - \frac{C_0(1-\alpha)}{(2\pi)^3}\int_{-\infty}^{\infty}\int_{-\infty}^{\infty}\int_{-\infty}^{\infty} \left|\hat{U}(\mathbf{k})\right|^2 \exp(-\mathbf{k}^2 t)dk_1\ dk_2\,dk_3 \tag{13}$$

with $\hat{U}(\mathbf{k})$ defined in Eq. (10).

For the cylindrical V_{PB} (3D-model) Eq. (13) yields:

$$F(t) = \frac{\pi d^2 hC_0}{4}\left\{1-(1-\alpha)\left[1-e^{-d^2/(8Dt)}\left(I_0\left(\frac{d^2}{8Dt}\right)+I_1\left(\frac{d^2}{8Dt}\right)\right)\right]\times\left[\mathrm{erf}\left(\frac{h}{2\sqrt{Dt}}\right)+\sqrt{\frac{4Dt}{\pi h^2}}(e^{-h^2/(4Dt)}-1)\right]\right\} \tag{14}$$

where d is the diameter and h is the depth of the photobleached volume, respectively.

For the square prism V_{PB} (3D-model) Eq. (13) yields:

$$F(t) = a^2 hC_0\left\{1-(1-\alpha)\left[\mathrm{erf}\left(\frac{a}{2\sqrt{Dt}}\right)+\sqrt{\frac{4Dt}{\pi a^2}}(e^{-a^2/(4Dt)}-1)\right]^2\times\left[\mathrm{erf}\left(\frac{h}{2\sqrt{Dt}}\right)+\sqrt{\frac{4Dt}{\pi h^2}}(e^{-h^2/(4Dt)}-1)\right]\right\} \tag{15}$$

where a is the side of the square and h is the depth of the photobleached volume, respectively.

For the 2D-model equations for the total fluorescence are derived by considering double, instead of triple integrals in Eqs. (10) and (13) yielding:

$$F(t) = \frac{\pi d^2 C_0}{4}\left\{1-(1-\alpha)\left[1-e^{-d^2/(8Dt)}\left(I_0\left(\frac{d^2}{8Dt}\right)+I_1\left(\frac{d^2}{8Dt}\right)\right)\right]\right\} \tag{16}$$

$$F(t) = a^2 C_0\left\{1-(1-\alpha)\left[\mathrm{erf}\left(\frac{a}{2\sqrt{Dt}}\right)+\sqrt{\frac{4Dt}{\pi a^2}}(e^{-a^2/(4Dt)}-1)\right]^2\right\} \tag{17}$$

for the circular and square photobleaching areas, respectively.

The total fluorescence intensity recovery data was fitted to mathematical models using Scientist software (MicroMaths Scientific Software).

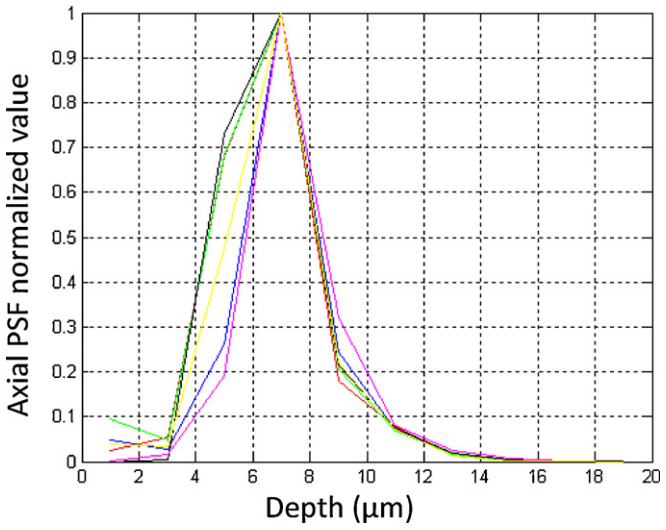

Fig. 1. Examples of the axial PSFs obtained by using a 63×, N.A. 1.3, water-immersion objective lens at six different sites.

3. Results and discussion

Examples of the axial PSF are presented in Fig. 1. The analysis of this data yielded the depth of the photobleaching volume of 2.7 ± 0.3 μm. In FRAP experiments, the lateral dimensions of the photobleached volume were selected to be close to the depth of a photobleached volume.

FRAP experiments for Rh:B in glycerol were performed using a cylindrical photobleached volume of diameter ≈ 2.5 μm. The fluorescence intensity recovery data were fitted using Eq. (14), resulting in the diffusion coefficient of $D = (3.2 \pm 0.5) \times 10^{-9}$ cm^2 s^{-1} ($n = 3$). The value of the diffusion coefficient of Rh:B in glycerol can also be approximated using empirical Wilke–Chang relationship (Wilke and Chang, 1955):

$$D = 7.4 \times 10^{-8}\frac{TM^{1/2}}{\eta V^{0.6}} \tag{18}$$

where D is in cm^2 s^{-1}, T is the temperature (=298 K) at which the diffusion coefficient is measured, M is the molecular weight of the glycerol (92 g mol^{-1}) and η is the dynamic viscosity of glycerol (934 centipoise, from Wolfram Alpha). Further, V is the molar volume of Rh:B at the normal boiling point, which was estimated as MW/ρ, where ρ (≈1 g cm^{-3}, from Wolfram Alpha), and MW (=479 g mol^{-1}) is the molecular weight of the Rh:B. Using these values in Eq. (18), yields $D \approx 5.6 \times 10^{-9}$ cm^2 s^{-1}, which is reasonably close to the value obtained from the fitting of the FRAP data ($3.2 \times 10^{-9} \pm 0.5$ cm^2 s^{-1}), considering that Eq. (18) is only an approximation. It can therefore be concluded that the FRAP experiments of the Rh:B in glycerol yielded reasonable value for the diffusion coefficient.

In Fig. 2, Z-stack FMT image set of the SC is presented, with images (a)–(e) acquired from closer to the surface of the SC to more in-depth layers of the SC at an interval of 1 μm. In images (b)–(d), a circular photobleached area is apparent, consistent with the cylindrical photobleached volume. The 3D-data from the Z-stack FMT image sets similar to that presented in Fig. 2 allows

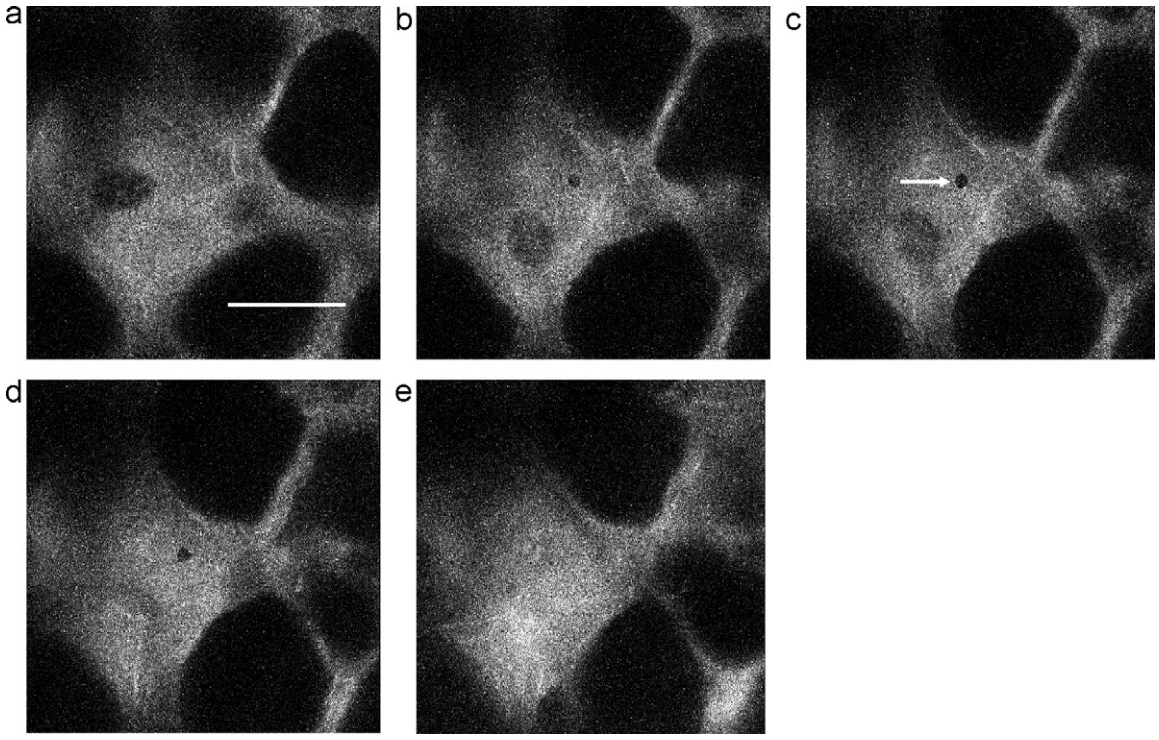

Fig. 2. Z-stack FMT image set of the SC with a cylindrical photobleaching volume evident as a dark circle pointed by a white arrow in image (c). Images (a)–(e) are from closer to the surface of the SC to more in-depth layers of the SC at an interval of 1 μm. Scale bar is 30 μm.

determination of the local structure of the SC phases (corneocytes and lipids) around the photobleached volume. For example, it can be seen in Fig. 2 that corneocytes appear as areas of little Rh:B fluorescence and lipid phase as bright Rh:B fluorescence. In principle, using this information it would be possible to construct a numerical finite-element model of the SC for each individual instance of FRAP experiment. While we understand that this type of mathematical modelling would represent a gold standard, in this work, we consider it appropriate to make simplifying assumptions that would give an analytical solution for the total fluorescence. We based the first mathematical model for the SC FRAP experiments on the assumption that the diffusion medium is infinite (referred to as the 3D-model). This assumption would have been valid, if the diffusion coefficient, as well as solubility, were the same in both the lipid and corneocyte phases of the SC. The second model is based on the assumption that diffusion occurs only in the lipid phase of the SC, and this phase is structured as an infinite layer sandwiched between two corneocyte layers (referred to as the 2D-model). This solution approximates the situation when corneocytes are impermeable to Rh:B or the concentration of Rh:B in them is negligible (due to, for example, low solubility). The real scenario is probably somewhere in between these two extreme cases, but given the fact that corneocytes have little Rh:B fluorescence (see Fig. 2), possibly closer to that of the 2D-model.

The square prism photobleached volume was used in SC FRAP experiments with the side of the square set to 2 μm. An example of the data of the total fluorescence versus time and its regressions with the 2D- and 3D-models is shown in Fig. 3. It can be seen that the quality of the regression is very good for both 2D- and 3D-models, which yield very similar curves. The value of the diffusion coefficient estimated by fitting the 3D-model (Eq. (15)) to the experimental data ($n=6$) was $3.5 \pm 1.0 \times 10^{-9}\,\mathrm{cm^2\,s^{-1}}$. The 2D-model (Eq. (17)) yielded the diffusion coefficient of $6.3 \pm 1.7 \times 10^{-9}\,\mathrm{cm^2\,s^{-1}}$. It can be noted that the values for the two distinct models differ by less than a factor of 2, yielding reasonably narrow range for the value of the diffusion coefficient of Rh:B in SC lipid phase. Both of these values are substantially less than the value of the diffusion coefficient for a similar molecular weight fluorophore (4a-diaza-s-indacene-3-hexadecanoic acid, $MW=474$) found by Johnson et al. (1996) ($D=19.2 \pm 1.7 \times 10^{-9}\,\mathrm{cm^2\,s^{-1}}$). In their work, the FRAP technique was used to measure a solute diffusion coefficient in artificial lipid bi-layers prepared from a dimyristoyl-phosphatidylcholine/cholesterol (40 mol%) mixture. This difference in values for the diffusion coefficients could be in part due to the higher temperature of the authors' experiments: 27 °C, compared to our experiments conducted at room temperature (22–25 °C). The value of the diffusion coefficient can be influenced by the lipid-fluorophore molecular interactions,

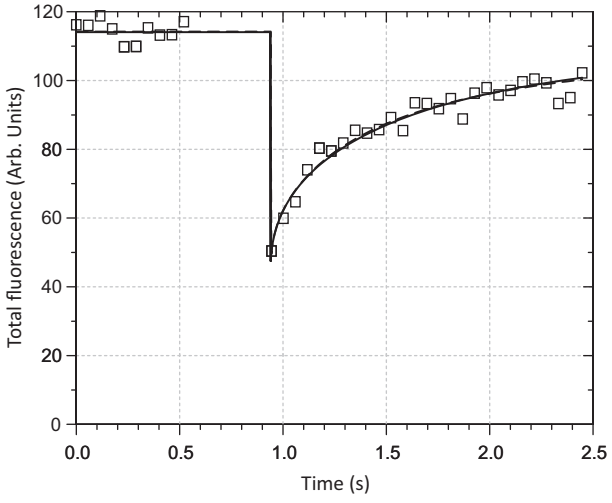

Fig. 3. Total fluorescence versus time data for SC (squares) and its regressions with the 2D (dashed line) and 3D models (solid line).

which are different for two fluorophores considered. Another possibility is that the structure of natural SC lipid bi-layers slows diffusion compared to that of the artificial lipid bi-layers used in the experiments reported by Johnson et al. (1996).

Since corneocytes appear as areas of little Rh:B fluorescence (see Fig. 2), FRAP experiments in the corneocyte phase of the SC have not yielded useful data. It is expected, though, that an appropriate selection of fluorophore, exhibiting measurable fluorescence in the corneocyte phase should allow determination of the value of the diffusion coefficient in this phase. It can be also argued that if coenocytes are not permeable or have little fluorophore present (corresponding to 2D-model case) the diffusion measured by the presented FRAP technique is the lateral diffusion in the lipid layers. Indeed, due to lipid layers orientation (parallel to corneocyte's surface) diffusion in these layers will happen in the lateral direction only (sandwiched between two corneocytes above and below) and, only the lateral diffusion in the lipid layers is likely to be measured by this technique. If fluorophore can be selected so that it is present in the coenocyte as well as corneocyte's wall being permeable to the fluorophore (this corresponds to our 3D-model), then molecular transport above and below the photo-bleached volume will be trans-lipid layer diffusion (as well as trans corneocyte wall), and should allow determination of the trans-lipid layer diffusion coefficient as well.

4. Conclusion

A FRAP method for determining local values of diffusion coefficient in SC was developed. The method was, first, verified using the simplified system of Rh:B in glycerol solution followed by application to human SC. For Rh:B fluorophore in SC FRAP it was found that only the diffusion coefficient in SC lipids can be determined from SC FRAP experiments. It was hypothesised that extending the SC FMT FRAP method to different fluorophores can yield local diffusion coefficients in both lipid and corneocyte phases.

Acknowledgements

We acknowledge the support by the NHMRC of Australia. We are grateful to Dr Tony O'Connor for discussions on applying Parseval's theorem to obtain analytical expression for the fluorescence recovery function.

References

Anissimov, Y.G., Roberts, M.S., 2004. Diffusion modeling of percutaneous absorption kinetics: 3. Variable diffusion and partition coefficients, consequences for stratum corneum depth profiles and desorption kinetics. Pharm. Sci. 93, 470–487.

Anissimov, Y.G., Roberts, M.S., 2009. Diffusion modeling of percutaneous absorption kinetics: 4. Effects of a slow equilibration process within stratum corneum on absorption and desorption kinetics. J. Pharm. Sci. 98, 772–781.

Braeckmans, K., Peeters, L., Sanders, N.N., De Smedt, S.C., Demeester, J., 2003. Three-dimensional fluorescence recovery after photobleaching with the confocal scanning laser microscope. Biophys. J. 85, 2240–2252.

Braga, J., Desterro, J.M., Carmo-Fonseca, M., 2004. Intracellular macromolecular mobility measured by fluorescence recovery after photobleaching with confocal laser scanning microscopes. Mol. Biol. Cell 15, 4749–4760.

Bunge, A.L., Guy, R.H., Hadgraft, J., 1999. The determination of a diffusional pathlength through the stratum corneum. Int. J. Pharm. 188, 121–124.

Johnson, M.E., Berk, D.A., Blankschtein, D., Golan, D.E., Jain, R.K., Langer, R.S., 1996. Lateral diffusion of small compounds in human stratum corneum and model lipid bilayer systems. Biophys. J. 71, 2656–2668.

Kasting, G.B., Barai, N.D., Wang, T.F., Nitsche, J.M., 2003. Mobility of water in human stratum corneum. J. Pharm. Sci. 92, 2326–2340.

Keister, J.C., Kasting, G.B., 1986. Use of transient diffusion to investigate transport pathways through skin. J. Control. Release 4, 111–117.

Kligman, A.M., Christophers, E., 1963. Preparation of isolated sheets of human stratum corneum. Arch. Dermatol. 88, 702–705.

Mitragotri, S., Anissimov, Y.G., Bunge, A.L., Frasch, H.F., Guy, R.H., Hadgraft, J., Kasting, G.B., Lane, M.E., Roberts, M.S., 2011. Mathematical models of skin permeability: an overview. Int. J. Pharm.

Roberts, M.S., Anissimov, Y.G., 2005. Mathematical models in percutaneous absorption. In: Bronaugh, R.L., Maibach, H.I. (Eds.), Percutaneous Absorption Drugs – Cosmetics – Mechanisms – Methodology. Marcel Dekker, New York, pp. 1–44.

Sniekers, Y.H., van Donkelaar, C.C., 2005. Determining diffusion coefficients in inhomogeneous tissues using fluorescence recovery after photobleaching. Biophys. J. 89, 1302–1307.

Wang, T.F., Kasting, G.B., Nitsche, J.M., 2006. A multiphase microscopic diffusion model for stratum corneum permeability. I. Formulation, solution, and illustrative results for representative compounds. J. Pharm. Sci. 95, 620–648.

Wang, T.F., Kasting, G.B., Nitsche, J.M., 2007. A multiphase microscopic diffusion model for stratum corneum permeability. II. Estimation of physicochemical parameters, and application to a large permeability database. J. Pharm. Sci. 96, 3024–3051.

Wilke, C.R., Chang, P., 1955. Correlation of diffusion coefficients in dilute solutions. AIChE J. 1, 264–270.

Wu, Y., Anissimov, Y.G., Roberts, M.S., 2011. Introduction to dermatokinetics. In: Murthy, S.N. (Ed.), Dermatokinetics of Therapeutic Agents. CRC Press, Boca Raton, pp. 1–23.